 CMES, vol.28, no.1, pp.57-76, 2008

Thermal Bending of Reissner-Mindlin Plates by the MLPG

J. Sladek[1], V. Sladek[1], P. Solek[2] and P.H. Wen[3]

Abstract: A meshless local Petrov-Galerkin (MLPG) method is applied to solve thermal bending problems described by the Reissner-Mindlin theory. Both stationary and thermal shock loads are analyzed here. Functionally graded material properties with continuous variation in the plate thickness direction are considered here. The Laplace-transformation is used to treat the time dependence of the variables for transient problems. A weak formulation for the set of governing equations in the Reissner-Mindlin theory is transformed into local integral equations on local subdomains in the mean surface of the plate by using a unit test function. Nodal points are randomly spread on the surface of the plate and each node is surrounded by a circular subdomain to which local integral equations are applied. The meshless approximation based on the Moving Least-Squares (MLS) method is employed for the implementation.

Keyword: Local boundary integral equations, Laplace-transform, Stehfest's inversion, MLS approximation, functionally graded material, orthotropic properties

1 Introduction

Plate structures are widely used in many engineering structures such as aircraft, civil and ship engineering. Plates are often subjected to combinations of lateral pressure and thermal loading. However, many linear bending studies are focused only to a lateral pressure load with assumption of uniformly distributed temperature in the whole plate. The first attempt to analyze thin plates under a thermal load was made by Marguerre (1935). A nice introduction and overview of pioneering efforts was given by Boley and Weiner (1960). Later Das and Navaratna (1962) investigated simply supported plates with temperature distribution symmetric to the middle surface. Investigations dealing with static and dynamic behaviour of isotropic and anisotropic thermoelastic plates have been discussed by Tauchert (1986, 1987). Analytical solution for thermal bending of thin, anisotropic, clamped elliptic plates is given by Laura and Rossit (1999). Kamiya et al. (1981) introduced the boundary integral equation method to analyze thermal bending problems. De Leon and Paris (1987) developed a boundary element method based on the decomposition of Kirchhoff's governing equation for plate deflection into a pair of harmonic equations. Results are presented for a simply supported isotropic plate with linear variation of temperature through the plate thickness. A global method of generalized differential quadrature for large deflections of thin plates under a thermal load is given by Lin et al. (1994). Tauchert (1991) gave a nice overview of thermally induced flexure, buckling and vibration of plates described by the Kirchhoff theory.

Among many thick plate theories available, those of Reissner (1946), Mindlin (1951) and higher order shear theories [Reddy, 1997] are widely accepted and have found applications of many engineering problems. Thermoelastic analyses including transverse shear effects were performed by Das and Rath (1972) and Bapu Rao (1979). Reddy and Hsu (1980) presented analytical solution for simply supported rectangular cross-ply laminated plates under sinusoidal mechanical load and temperature assumed to vary linearly through the thickness. Rolfes et al (1998) stud-

[1] Institute of Construction and Architecture, Slovak Academy of Sciences, 84503 Bratislava, Slovakia
[2] Department of Mechanics, Slovak Technical University, Bratislava, Slovakia
[3] School of Engineering and Materials Sciences, Queen Mary University of London, Mile End, London E14NS, U.K.

ied both the transverse shear and normal stresses in laminated plates subjected to mechanical and thermal loads. The analysis is based on the first-order shear deformation theory and the plate is discretized by using a single field displacement finite element model. Nonlinear analysis of simply supported Reissner-Mindlin plates subjected to lateral pressure and thermal loading and resting on two-parameter elastic foundations is given by Shen (2000). Suetake (2006) modified high-order bending theory of plates by constitution of the lateral loads through consideration of the transverse normal stress. The effects of shear deformation and rotatory inertia following Reissner-Mindlin's deformation theory are included in the elastoplastic transient response of plates with all possible boundary conditions on edges and any interior support conditions such as isolated points (columns), lines (walls) or regions (patches) by Providakis (2007). Wen and Hon (2007) used smooth radial basis functions for the geometrically nonlinear analysis of Reissner-Mindlin plate.

Recently, functionally graded materials (FGMs) have been extensively used for engineering structures under a severe thermal load. FGMs are multi-phase materials with the phase volume fractions varying gradually in space, in a predetermined profile. This results in continuously graded thermomechanical properties at the (macroscopic) structural scale with superior material properties. FGMs posses some advantages over conventional composites because of their continuously graded structures and properties [Suresh and Mortensen, 1998; Miyamoto et al., 1999]. FGMs may exhibit isotropic or anisotropic material properties, depending on the processing technique and the practical engineering requirements. Due to the high mathematical complexity of the initial-boundary value problems, analytical approaches for the FGM bodies are restricted to simple geometry and boundary conditions. Thus, analyses in FGM demand accurate and efficient numerical methods. Praveen and Reddy (1998) analyzed the thermomechanical response of thick plates with continuous variation of properties through the plate thickness. The FEM has been applied to isotropic plates with a simple power law distribution of ceramic and metallic constituents. Vel and Batra (2002) obtained an exact solution for three-dimensional deformations of a simply supported functionally graded rectangular plates subjected to mechanical and thermal loads on its top and bottom surfaces.

Meshfree techniques for solving PDE in physics and engineering are a powerful new alternative to the traditional mesh-based techniques. Focusing only on nodes or points instead of elements used in the conventional FEM or BEM, meshless approaches have certain advantages. One of the most rapidly developed meshfree methods is the Meshless Local Petrov-Galerkin method. The MLPG method has attracted much attention during the past decade [Atluri and Shen, 2002; Atluri, 2004; Han et al., 2003; Mikhailov, 2002; Sellountos et al., 2005] for many problems of continuum mechanics. Recent successes of the MLPG methods have been reported in solving a 4^{th} order ordinary differential equation [Atluri and Shen (2005)]; in analyzing vibrations of a beam with multiple cracks [Andreaus et al (2005)]; in simulation of water waves [Ma (2005)]; in the development of a nonlinear formulation of the MLPG finite-volume mixed method for the large deformation analysis of static and dynamic problems [Han et al (2005)]; in simplified treatment of essential boundary conditions by a novel modified MLS procedure [Gao et al (2006)]; in application to solving the Q-tensor equations of nematostatics [Pecher et al (2006)]; in analysis of transient thermomechanical response of functionally gradient composites [Ching and Chen (2006)]; in the ability for solving high-speed contact, impact and penetration problems with large deformations and rotations [Han et al (2006)]; in the development of the mixed scheme to interpolate the elastic displacements and stresses independently [Atluri et al (2006a), (2006b)]; in proposal of a direct solution method for the quasi-unsymmetric sparse matrix arising in the MLPG [Yuan et al (2007)]; in modelling nonlinear water waves [Ma (2007)]; in the development of the MLPG with using the Dirac delta function as the test function for 2D heat conduction problems in irregular domain

[Wu et al (2007)]; for studying the diffusion of a magnetic field within a non-magnetic conducting medium with nonhomogeneous and anisotropic electrical resistivity [Johnoson and Owen (2007)]; in the development of the MLPG with using simplified finite difference interpolation [Ma (2008)].

In the present paper, the authors have developed a meshless method based on the local Petrov-Galerkin weak-form to solve thermal problems of orthotropic thick plates with material properties continuously varying through the plate thickness. The Reissner-Mindlin theory reduces the original 3-d thick plate problem to a 2-d problem. In our meshless method, nodal points are randomly distributed over the mean surface of the considered plate. Each node is the center of a circle surrounding this node. Similar approach has been successfully applied to a thin Kirchhoff plate [Sladek et al., 2002, 2003] where the governing equation is decomposed into two partial differential equations (PDEs) of the second order [De Leon and Paris, 1987]. Long and Atluri (2002) applied the meshless local Petrov Galerkin method to solve the bending problem of a thin plate. The MLPG method has been also applied to Reissner-Mindlin plates under dynamic load by Sladek et al. (2007). Soric et al. (2004) have performed a three-dimensional analysis of thick plates, where a plate is divided by small cylindrical subdomains for which the MLPG is applied. Homogeneous material properties of plates are considered in previous papers. Recently, Qian et al. (2004) extended the MLPG for 3-D deformations in thermoelastic bending of functionally graded isotropic plates.

In this paper the Laplace-transform technique is applied to the set of governing differential equations for elastodynamic Reissner-Mindlin plate bending theory with Duhamel-Neumann constitutive equations. Unknown Laplace-transformed quantities on the local boundaries are determined by the local boundary integral equations. A unit test function is used in the local weak-form. Applying the Gauss divergence theorem to the weak-form, the local boundary-domain integral equations are derived. The numerical integration of the domain integrals arising from the inertial term and the initial values on a simple domain does not give rise to difficulties if the meshless approximation based on the Moving Least-Squares (MLS) method is applied. Temperature distribution in plate has to be analyzed as 3-D problem. The MLPG is applied to transient heat conduction equations. The Laplace transform technique is used to eliminate time variable too. Several quasi-static boundary value problems must be solved for various values of the Laplace-transform parameter. The Stehfest's inversion method [Stehfest, 1970] is applied to obtain the time-dependent solution.

Numerical results for simply supported and clamped square plates with a uniform or sinusoidal temperature distribution on the top surface of the plate are presented to illustrate the accuracy and efficiency of the proposed method. A thermal shock with Heaviside time variation on the top surface of the simply supported plate is also analyzed. Comparisons of the present numerical results with FEM results show good agreement.

2 Local integral equations for Reissner-Mindlin plate theory

Consider an elastic orthotropic plate of constant thickness h, with the mean surface occupying the domain Ω in the plane (x_1, x_2). The plate is subjected to thermal loading with the temperature field $\theta(\mathbf{x}, x_3, t)$. The Reissner-Mindlin plate bending theory [Reissner, 1946; Mindlin, 1951] is used to describe the plate deformation. The transverse shear strains are represented as constant throughout the plate thickness and some correction coefficients are required for computation of transverse shear forces in that theory. Then, the spatial displacement field, due to transverse loading and expressed in terms of displacement components u_1, u_2, and u_3, has the following form [Reddy, 1997]

$$\begin{aligned} u_1(\mathbf{x},t) &= x_3 w_1(\mathbf{x},t) \\ u_2(\mathbf{x},t) &= x_3 w_2(\mathbf{x},t) \\ u_3(\mathbf{x},t) &= w_3(\mathbf{x},t), \end{aligned} \tag{1}$$

where $w_\alpha(x_1, x_2, t)$ and $w_3(x_1, x_2, t)$ represent the rotations around the in-plane axes and the out-of-plane deflection, respectively (Fig. 1).

The linear strains are given by

$$\begin{aligned}
\varepsilon_{11}(\mathbf{x},t) &= x_3 w_{1,1}(\mathbf{x},t) \\
\varepsilon_{22}(\mathbf{x},t) &= x_3 w_{2,2}(\mathbf{x},t) \\
\varepsilon_{12}(\mathbf{x},t) &= x_3 (w_{1,2}(\mathbf{x},t) + w_{2,1}(\mathbf{x},t))/2. \\
\varepsilon_{13}(\mathbf{x},t) &= (w_1(\mathbf{x},t) + w_{3,1}(\mathbf{x},t))/2. \\
\varepsilon_{23}(\mathbf{x},t) &= (w_2(\mathbf{x},t) + w_{3,2}(\mathbf{x},t))/2.
\end{aligned} \tag{2}$$

In the case of orthotropic materials, the relation between the stress σ_{ij} and the strain ε_{ij} when temperature changes are considered, is governed by the well known Duhamel-Neumann constitutive equations for the stress tensor

$$\sigma_{ij}(\mathbf{x},t) = c_{ijkl}\varepsilon_{kl}(\mathbf{x},t) - \gamma_{ij}\theta(\mathbf{x},x_3,t) \tag{3}$$

where c_{ijkl} are the material stiffness coefficients. The stress-temperature modulus can be expressed through the stiffness coefficients and the coefficients of linear thermal expansion α_{kl}

$$\gamma_{ij} = c_{ijkl}\alpha_{kl}. \tag{4}$$

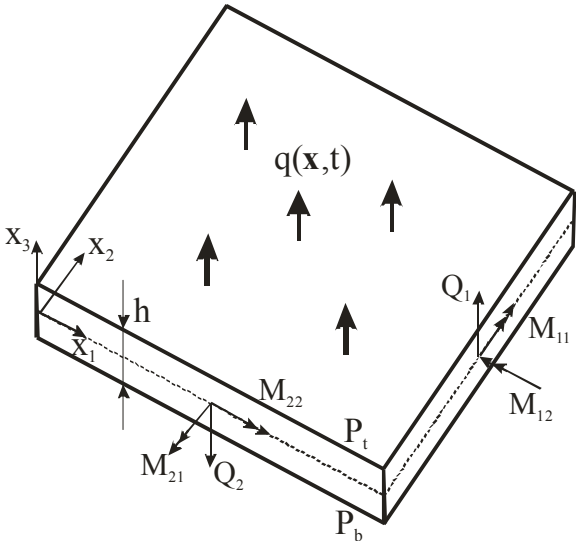

Figure 1: Sign convention of bending moments and forces for FGM plate

For plane problems the constitutive equation (3) is frequently written in terms of the second-order tensor of elastic constants [Lekhnitskii (1963)].

The constitutive equation for orthotropic materials and plane stress problem has the following form

$$\begin{bmatrix} \sigma_{11} \\ \sigma_{22} \\ \sigma_{12} \\ \sigma_{13} \\ \sigma_{23} \end{bmatrix} = \mathbf{G}(\mathbf{x}) \begin{bmatrix} \varepsilon_{11} \\ \varepsilon_{22} \\ 2\varepsilon_{12} \\ 2\varepsilon_{13} \\ 2\varepsilon_{23} \end{bmatrix} - \begin{bmatrix} \gamma_{11} \\ \gamma_{22} \\ 0 \\ 0 \\ 0 \end{bmatrix} \theta(\mathbf{x},x_3,t) \tag{5}$$

where

$$\mathbf{G}(\mathbf{x}) = \begin{bmatrix} E_1/e & E_1\nu_{21}/e & 0 & 0 & 0 \\ E_2\nu_{12}/e & E_2/e & 0 & 0 & 0 \\ 0 & 0 & G_{12} & 0 & 0 \\ 0 & 0 & 0 & G_{13} & 0 \\ 0 & 0 & 0 & 0 & G_{23} \end{bmatrix}$$

with $e = 1 - \nu_{12}\nu_{21}$. E_α are the Young's moduli refering to the axes x_α , $\alpha = 1, 2$, G_{12} , G_{13} and G_{23} are shear moduli, $\nu_{\alpha\beta}$ are Poisson's ratios.

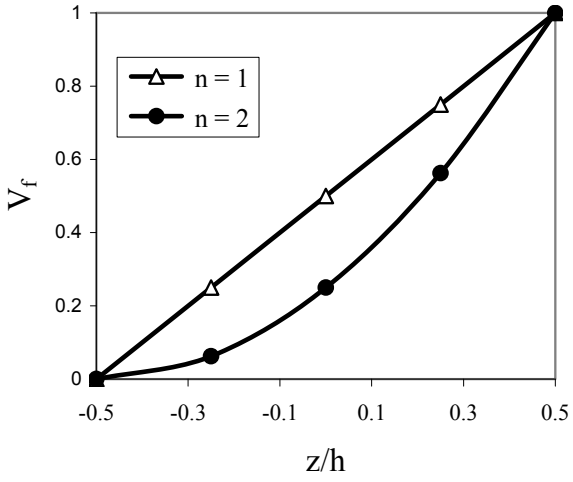

Figure 2: Variation of volume fraction over the plate thickness, for linear and quadratic power-law index

Next, we assume that the material properties are graded along the plate thickness, and we represent the profile for volume fraction variation by

$$P(x_3) = P_b + (P_t - P_b)V$$
$$\text{with } V = \left(\frac{x_3}{h} + \frac{1}{2}\right)^n, \tag{6}$$

where P denotes a generic property like modulus, P_t and P_b denote the property of the top and bottom faces of the plate, respectively, and n is a parameter that dictates the material variation profile (Fig. 2). Poisson ratios are assumed to be uniform.

The bending moments $M_{\alpha\beta}$ and the shear forces Q_α are defined as

$$\begin{bmatrix} M_{11} \\ M_{22} \\ M_{12} \end{bmatrix} = \int_{-h/2}^{h/2} \begin{bmatrix} \sigma_{11} \\ \sigma_{22} \\ \sigma_{12} \end{bmatrix} x_3 dx_3 \qquad \begin{bmatrix} Q_1 \\ Q_2 \end{bmatrix} = \kappa \int_{-h/2}^{h/2} \begin{bmatrix} \sigma_{13} \\ \sigma_{23} \end{bmatrix} dx_3, \tag{7}$$

where $\kappa = 5/6$ in the Reissner plate theory.

Substituting equations (5) and (2) into moment and force resultants (7) allows the expression of the bending moments $M_{\alpha\beta}$ and shear forces Q_α for α,β=1,2, in terms of rotations, lateral displacements of the orthotropic plate and temperature. In the case of considered continuous gradation of material properties through the plate thickness, one obtains

$$\begin{aligned} M_{\alpha\beta} &= D_{\alpha\beta}\left(w_{\alpha,\beta} + w_{\beta,\alpha}\right) + C_{\alpha\beta} w_{\gamma,\gamma} - H_{\alpha\beta} \\ Q_\alpha &= C_\alpha \left(w_\alpha + w_{3,\alpha}\right), \end{aligned} \tag{8}$$

where

$$H_{\alpha\beta} = \int_{-h/2}^{h/2} x_3 \gamma_{\alpha\beta} \theta(\mathbf{x}, x_3, t) dx_3.$$

In eq. (8), repeated indices α, β do not imply summation, and the material parameters $D_{\alpha\beta}$ and $C_{\alpha\beta}$ are given as

$$\begin{aligned} &D_{11} = \frac{D_1}{2}(1-\nu_{21}), \quad D_{22} = \frac{D_2}{2}(1-\nu_{12}), \\ &D_{12} = D_{21} = \frac{\overline{G}_{12} h^3}{12}, \\ &C_{11} = D_1 \nu_{21}, \quad C_{22} = D_2 \nu_{12}, \quad C_{12} = C_{21} = 0, \\ &D_\alpha = \frac{\overline{E}_\alpha h^3}{12e}, \quad D_1 \nu_{21} = D_2 \nu_{12}, \quad C_\alpha = \kappa h \overline{G}_{\alpha 3}, \end{aligned} \tag{9}$$

where

$$\overline{E}_\alpha \equiv \begin{cases} E_{\alpha t} = E_{\alpha b}, & n = 0 \\ (E_{\alpha b} + E_{\alpha t})/2, & n = 1 \\ (3E_{\alpha b} + 2E_{\alpha t})/5, & n = 2 \end{cases}$$

$$\overline{G}_{12} \equiv \begin{cases} G_{12t} = G_{12b}, & n = 0 \\ (G_{12b} + G_{12t})/2, & n = 1 \\ (3G_{12b} + 2G_{12t})/5, & n = 2 \end{cases}$$

$$\overline{G}_{\alpha 3} \equiv \begin{cases} G_{\alpha 3t} = G_{\alpha 3b}, & n = 0 \\ (G_{\alpha 3b} + G_{\alpha 3t})/2, & n = 1 \\ (2G_{\alpha 3b} + G_{\alpha 3t})/3, & n = 2 \end{cases}$$

with the same meaning of subscripts b and t as in Eq.(6).

For a general variation of material properties through the plate thickness:

$$D_{11} = \int_{-h/2}^{h/2} x_3^2 E_1(x_3) \frac{1-\nu_{21}}{e} dx_3$$

$$D_{22} = \int_{-h/2}^{h/2} x_3^2 E_2(x_3) \frac{1-\nu_{12}}{e} dx_3$$

$$D_{12} = \int_{-h/2}^{h/2} x_3^2 G_{12}(x_3) dx_3$$

$$C_{11} = \int_{-h/2}^{h/2} x_3^2 E_1(x_3) \frac{\nu_{21}}{e} dx_3$$

$$C_{22} = \int_{-h/2}^{h/2} x_3^2 E_2(x_3) \frac{\nu_{12}}{e} dx_3$$

$$C_\alpha = \kappa \int_{-h/2}^{h/2} G_{\alpha 3}(x_3) dx_3$$

Using the Reissner's linear theory of thick plates [Reissner, 1946], the equations of motion may be written as

$$\begin{aligned} &M_{\alpha\beta,\beta}(\mathbf{x},t) - Q_\alpha(\mathbf{x},t) = \frac{\rho h^3}{12} \ddot{w}_\alpha(\mathbf{x},t), \\ &Q_{\alpha,\alpha}(\mathbf{x},t) = \rho h \ddot{w}_3(\mathbf{x},t), \quad \mathbf{x} \in \Omega, \end{aligned} \tag{10}$$

where ρ is the mass density, and throughout the paper Greek indices vary from 1 to 2. The dots over a quantity indicate differentiations with respect to time t.

To eliminate the time variable t in the governing equations (10), the Laplace-transform is applied

$$L[f(\mathbf{x},t)] = \overline{f}(\mathbf{x},s) = \int_0^\infty f(\mathbf{x},t) e^{-st} dt\,.$$

Then, one obtains

$$\overline{M}_{\alpha\beta,\beta}(\mathbf{x},s)-\overline{Q}_{\alpha}(\mathbf{x},s) = \frac{\rho h^3}{12}s^2\overline{w}_{\alpha}(\mathbf{x},s)-\overline{R}_{\alpha}(\mathbf{x},s), \quad (11)$$

$$\overline{Q}_{\alpha,\alpha}(\mathbf{x},s)=\rho h s^2\overline{w}_3(\mathbf{x},s)-\overline{R}_3(\mathbf{x},s), \quad (12)$$

where s is the Laplace-transform parameter, while $\overline{R}_{\alpha}$ and $\overline{R}_3$ are given by

$$\overline{R}_{\alpha}(\mathbf{x},s)=\frac{\rho h^3}{12}\left[sw_{\alpha}(\mathbf{x})+\dot{w}_{\alpha}(\mathbf{x})\right],$$

$$\overline{R}_3(\mathbf{x},s)=\rho h s w_3(\mathbf{x})+\rho h\dot{w}_3(\mathbf{x}),$$

with $w_{\alpha}(\mathbf{x})$, $w_3(\mathbf{x})$, $\dot{w}_{\alpha}(\mathbf{x})$ and $\dot{w}_3(\mathbf{x})$ being the initial values and the initial velocities of the generalized displacement field.

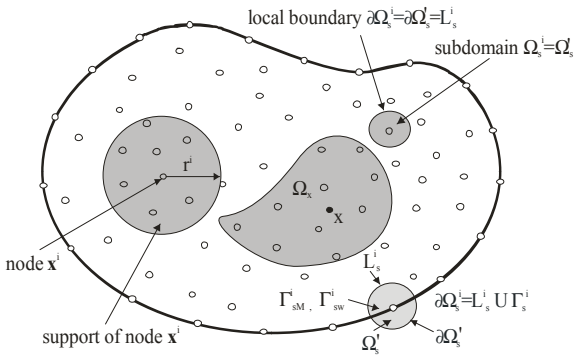

Figure 3: Local boundaries for weak formulation, the domain Ω_x for MLS approximation of the trial function, and support area of weight function around node $\mathbf{x}^i$

Instead of writing the global weak-form for the above governing equations, the MLPG methods construct the weak-form over local subdomains such as Ω_s, which is a small region taken for each node inside the global domain [Atluri, 2004]. The local subdomains overlap each other and cover the whole global domain Ω (Fig. 3). The local subdomains could be of any geometrical shape and size. In the current paper, the local subdomains are taken to be of circular shape. The local weak-form of the governing equations (11) and (12) for $\mathbf{x}^i\in\Omega_s^i$ can be written as

$$\int_{\Omega_s^i}\left[\overline{M}_{\alpha\beta,\beta}(\mathbf{x},s)-\overline{Q}_{\alpha}(\mathbf{x},s)-\frac{\rho h^3}{12}s^2\overline{w}_{\alpha}(\mathbf{x},s) +\overline{R}_{\alpha}(\mathbf{x},s)\right]w^*_{\alpha\gamma}(\mathbf{x})d\Omega=0, \quad (13)$$

$$\int_{\Omega_s^i}\left[\overline{Q}_{\alpha,\alpha}(\mathbf{x},s)-\rho h s^2\overline{w}_3(\mathbf{x},s) +\overline{R}_3(\mathbf{x},s)\right]w^*_3(\mathbf{x})d\Omega=0, \quad (14)$$

where $w^*_{\alpha\beta}(\mathbf{x})$ and $w^*(\mathbf{x})$ are weight or test functions.

Applying the Gauss divergence theorem to Eqs. (13) and (14) one obtains

$$\int_{\partial\Omega_s^i}\overline{M}_{\alpha}(\mathbf{x},s)u^*_{\alpha\gamma}(\mathbf{x})d\Gamma-\int_{\Omega_s^i}\overline{M}_{\alpha\beta}(\mathbf{x},s)u^*_{\alpha\gamma,\beta}(\mathbf{x})d\Omega -\int_{\Omega_s^i}\overline{Q}_{\alpha}(\mathbf{x},s)u^*_{\alpha\gamma}(\mathbf{x})d\Omega -\int_{\Omega_s^i}\frac{\rho h^3}{12}s^2\overline{w}_{\alpha}(\mathbf{x},s)u^*_{\alpha\gamma}(\mathbf{x})d\Omega +\int_{\Omega_s^i}\overline{R}_{\alpha}(\mathbf{x},s)u^*_{\alpha\gamma}(\mathbf{x})d\Omega=0, \quad (15)$$

$$\int_{\partial\Omega_s^i}\overline{Q}_{\alpha}(\mathbf{x},s)n_{\alpha}(\mathbf{x})u^*(\mathbf{x})d\Gamma-\int_{\Omega_s^i}\overline{Q}_{\alpha}(\mathbf{x},s)u^*_{,\alpha}(\mathbf{x})d\Omega -\int_{\Omega_s^i}\rho h s^2\overline{w}_3(\mathbf{x},s)u^*(\mathbf{x})d\Omega+\int_{\Omega_s^i}\overline{R}_3(\mathbf{x},s)u^*(\mathbf{x})d\Omega =0, \quad (16)$$

where $\partial\Omega_s^i$ is the boundary of the local subdomain and

$$\overline{M}_{\alpha}(\mathbf{x},s)=\overline{M}_{\alpha\beta}(\mathbf{x},s)n_{\beta}(\mathbf{x})$$

is the Laplace-transform of the normal bending moment and n_{α} is the unit outward normal vector to the boundary $\partial\Omega_s^i$. The local weak-forms (15) and (16) are the starting point for deriving

local boundary integral equations on the basis of appropriate test functions. Unit step functions are chosen for the test functions $w^*_{\alpha\beta}(\mathbf{x})$ and $w^*(\mathbf{x})$ in each subdomain

$$w^*_{\alpha\gamma}(\mathbf{x}) = \begin{cases} \delta_{\alpha\gamma} & \text{at } \mathbf{x} \in (\Omega_s \cup \partial\Omega_s) \\ 0 & \text{at } \mathbf{x} \notin (\Omega_s \cup \partial\Omega_s) \end{cases}, \qquad w^*(\mathbf{x}) = \begin{cases} 1 & \text{at } \mathbf{x} \in (\Omega_s \cup \partial\Omega_s) \\ 0 & \text{at } \mathbf{x} \notin (\Omega_s \cup \partial\Omega_s) \end{cases}. \tag{17}$$

Then, the local weak-forms (15) and (16) are transformed into the following local boundary integral equations

$$\int_{\partial\Omega_s^i} \overline{M}_\alpha(\mathbf{x},s)d\Gamma - \int_{\Omega_s^i} \overline{Q}_\alpha(\mathbf{x},s)d\Omega - \int_{\Omega_s^i} \frac{\rho h^3}{12} s^2 \overline{w}_\alpha(\mathbf{x},s)d\Omega + \int_{\Omega_s^i} \overline{R}_\alpha(\mathbf{x},s)d\Omega = 0, \tag{18}$$

$$\int_{\partial\Omega_s^i} \overline{Q}_\alpha(\mathbf{x},s)n_\alpha(\mathbf{x})d\Gamma - \int_{\Omega_s^i} \rho h s^2 \overline{w}_3(\mathbf{x},s)d\Omega + \int_{\Omega_s^i} \overline{R}_3(\mathbf{x},s)d\Omega = 0. \tag{19}$$

In the above local integral equations, the trial functions $\overline{w}_\alpha(\mathbf{x},s)$, related to rotations, and $\overline{w}_3(\mathbf{x},s)$, related to displacements, are chosen as the moving least-squares (MLS) approximations over a number of nodes randomly spread within the domain of influence.

3 Numerical solution

In general, a meshless method uses a local interpolation to represent the trial function with the values (or the fictitious values) of the unknown variable at some randomly located nodes. The moving least-squares (MLS) approximation [Lancaster and Salkauskas, 1981; Nayroles et al., 1992; Belytschko, 1996] used in the present analysis may be considered as one of such schemes. Let us consider a sub-domain Ω_x of the problem domain Ω in the neighbourhood of a point $\mathbf{x}$ for the definition of the MLS approximation of the trial function around $\mathbf{x}$ (Fig. 3). To approximate the distribution of the Laplace-transform of the generalized displacements (rotations and deflection) in Ω_x over a number of randomly located nodes $\{\mathbf{x}^a\}, a = 1,2,\ldots,n$, the MLS approximant $\overline{w}_i^h(\mathbf{x},s)$ of $\overline{w}_i(\mathbf{x},s)$ is defined by

$$\overline{\mathbf{w}}^h(\mathbf{x},s) = \mathbf{p}^T(\mathbf{x})\tilde{\mathbf{a}}(\mathbf{x},s), \quad \forall \mathbf{x} \in \Omega_x \tag{20}$$

where $\overline{\mathbf{w}}^h = \left[\overline{w}_1^h, \overline{w}_2^h, \overline{w}_3^h\right]^T$, $\mathbf{p}^T(\mathbf{x}) = \left[p^1(\mathbf{x}), p^2(\mathbf{x}), \ldots, p^m(\mathbf{x})\right]$ is a complete monomial basis of order m, and $\tilde{\mathbf{a}}(\mathbf{x},s) = \left[\mathbf{a}^1(\mathbf{x},s), \mathbf{a}^2(\mathbf{x},s), ..., \mathbf{a}^m(\mathbf{x},s)\right]^T$ is composed of vectors $\mathbf{a}^j(\mathbf{x},s) = \left[a_1^j(\mathbf{x},s), a_2^j(\mathbf{x},s), a_3^j(\mathbf{x},s)\right]^T$ which are functions of the spatial co-ordinates $\mathbf{x} = [x_1, x_2]^T$ and the transform- parameter s.

The coefficient vector $\tilde{\mathbf{a}}(\mathbf{x},s)$ is determined by minimizing a weighted discrete L_2 -norm defined as

$$J(\mathbf{x}) = \sum_{a=1}^{n} v^a(\mathbf{x}) \left[\mathbf{p}^T(\mathbf{x}^a)\tilde{\mathbf{a}}(\mathbf{x},s) - \hat{\mathbf{w}}^a(s)\right]^2, \tag{21}$$

where $v^a(\mathbf{x}) > 0$ is the weight function associated with the node a and the square power is considered in the sense of scalar product. Recall that n is the number of nodes in Ω_x for which the weight function $v^a(\mathbf{x}) > 0$ and $\hat{\mathbf{w}}^a(s)$ are the fictitious nodal values, but not the nodal values of the unknown trial function $\overline{\mathbf{w}}^h(\mathbf{x},s)$ in general. The stationarity of Jin eq. (21) with respect to $\tilde{\mathbf{a}}(\mathbf{x},s)$ leads to

$$\mathbf{A}(\mathbf{x})\tilde{\mathbf{a}}(\mathbf{x},s) - \mathbf{B}(\mathbf{x})\hat{\mathbf{w}}(s) = 0, \tag{22}$$

where

$$\hat{\mathbf{w}}(s) = \left[\hat{\mathbf{w}}^1(s), \hat{\mathbf{w}}^2(s), ..., \hat{\mathbf{w}}^n(s)\right]^T$$

$$\mathbf{A}(\mathbf{x}) = \sum_{a=1}^{n} v^a(\mathbf{x})\mathbf{p}(\mathbf{x}^a)\mathbf{p}^T(\mathbf{x}^a),$$

$$\mathbf{B}(\mathbf{x}) = \left[v^1(\mathbf{x})\mathbf{p}(\mathbf{x}^1), v^2(\mathbf{x})\mathbf{p}(\mathbf{x}^2), ..., v^n(\mathbf{x})\mathbf{p}(\mathbf{x}^n)\right]. \tag{23}$$

The solution of eq. (22) for $\tilde{\mathbf{a}}(\mathbf{x},s)$ and the subsequent substitution into eq. (20) lead to the following expression

$$\overline{\mathbf{w}}^h(\mathbf{x},s)=\mathbf{\Phi}^T(\mathbf{x})\cdot\hat{\mathbf{w}}(s)=\sum_{a=1}^{n}\phi^a(\mathbf{x})\hat{\mathbf{w}}^a(s), \quad (24)$$

where

$$\mathbf{\Phi}^T(\mathbf{x})=\mathbf{p}^T(\mathbf{x})\mathbf{A}^{-1}(\mathbf{x})\mathbf{B}(\mathbf{x}). \quad (25)$$

In eq. (24), $\phi^a(\mathbf{x})$ is usually referred to as the shape function of the MLS approximation corresponding to the nodal point $\mathbf{x}^a$. From eqs. (23) and (25), it can be seen that $\phi^a(\mathbf{x})=0$ when $v^a(\mathbf{x})=0$. In practical applications, $v^a(\mathbf{x})$ is often chosen in such a way that it is non-zero over the support of the nodal point $\mathbf{x}_i$. The support of the nodal point $\mathbf{x}^a$ is usually taken to be a circle of the radius r_i centred at $\mathbf{x}^a$ (see Fig. 3). The radius r_i is an important parameter of the MLS approximation because it determines the range of the interaction (coupling) between the degrees of freedom defined at considered nodes.

A 4^{th}-order spline-type weight function is applied in the present work

$$v^a(\mathbf{x})=\begin{cases}1-6\left(\frac{d^a}{r^a}\right)^2+8\left(\frac{d^a}{r^a}\right)^3-3\left(\frac{d^a}{r^a}\right)^4 & 0\le d^a\le r^a\\ 0 & d^a\ge r^a\end{cases} \quad (26)$$

where $d^a=\|\mathbf{x}-\mathbf{x}^a\|$ and r^a is the radius of the circular support domain. With eq. (26), the C^1-continuity of the weight function is ensured over the entire domain, therefore the continuity condition of the bending moments and the shear forces is satisfied. The size of the support r^a should be large enough to cover a sufficient number of nodes in the domain of definition to ensure the regularity of the matrix $\mathbf{A}$. The value of n is determined by the number of nodes lying in the support domain with radius r^a .

The partial derivatives of the MLS shape functions are obtained as [Atluri, 2004]

$$\phi^a_{,k}=\sum_{j=1}^{m}\left[p^j_{,k}(\mathbf{A}^{-1}\mathbf{B})^{ja}+p^j(\mathbf{A}^{-1}\mathbf{B}_{,k}+\mathbf{A}^{-1}_{,k}\mathbf{B})^{ja}\right], \quad (27)$$

wherein $\mathbf{A}^{-1}_{,k}=\left(\mathbf{A}^{-1}\right)_{,k}$ represents the derivative of the inverse of $\mathbf{A}$ with respect to x_k , which is given by

$$\mathbf{A}^{-1}_{,k}=-\mathbf{A}^{-1}\mathbf{A}_{,k}\mathbf{A}^{-1}.$$

The directional derivatives of $\overline{\mathbf{w}}(\mathbf{x},s)$ are approximated in terms of the same nodal values as

$$\overline{\mathbf{w}}_{,k}(\mathbf{x},s)=\sum_{a=1}^{n}\hat{\mathbf{w}}^a(s)\phi^a_{,k}(\mathbf{x}). \quad (28)$$

Substituting the approximation (28) into the definition of the normal bending (7), one obtains for

$$\overline{\mathbf{M}}(\mathbf{x},s)=\left[\overline{M}_1(\mathbf{x},s),\,\overline{M}_2(\mathbf{x},s)\right]^T$$

$$\begin{aligned}\overline{\mathbf{M}}(\mathbf{x},s)&=\mathbf{N_1}\sum_{a=1}^{n}\mathbf{B}^a_1(\mathbf{x})\mathbf{w}^{*a}(s)\\ &+\mathbf{N_2}\sum_{a=1}^{n}\mathbf{B}^a_2(\mathbf{x})\mathbf{w}^{*a}(s)-\overline{\mathbf{H}}(\mathbf{x},s)\\ &=\mathbf{N}_\alpha(\mathbf{x})\sum_{a=1}^{n}\mathbf{B}^a_\alpha(\mathbf{x})\mathbf{w}^{*a}(s)-\overline{\mathbf{H}}(\mathbf{x},s),\end{aligned} \quad (29)$$

where the vector $\mathbf{w}^{*a}(s)$ is defined as a column vector $\mathbf{w}^{*a}(s)=[\hat{w}^a_1(s),\,\hat{w}^a_2(s)]^T$, the vector $\overline{\mathbf{H}}(\mathbf{x},s)=[\overline{H}_{11}n_1,\,\overline{H}_{22}n_2]^T$, the matrices $\mathbf{N}_\alpha(\mathbf{x})$ are related to the normal vector **n(x)** on $\partial\Omega_s$ by

$$\mathbf{N}_1(\mathbf{x})=\begin{bmatrix}n_1 & 0 & n_2\\ 0 & n_2 & n_1\end{bmatrix}$$

and

$$\mathbf{N}_2(\mathbf{x})=\begin{bmatrix}C_{11} & 0\\ 0 & C_{22}\end{bmatrix}\begin{bmatrix}n_1 & n_1\\ n_2 & n_2\end{bmatrix}$$

and the matrices $\mathbf{B}^a_\alpha$ are represented by the gradients of the shape functions as

$$\mathbf{B}^a_1(\mathbf{x})=\begin{bmatrix}2D_{11}\phi^a_{,1} & 0\\ 0 & 2D_{22}\phi^a_{,2}\\ D_{12}\phi^a_{,2} & D_{12}\phi^a_{,1}\end{bmatrix},$$

$$\mathbf{B}^a_2(\mathbf{x})=\begin{bmatrix}\phi^a_{,1} & 0\\ 0 & \phi^a_{,2}\end{bmatrix}.$$

The influence on the material gradation is incorporated in $C_{\alpha\beta}$ and $D_{\alpha\beta}$ defined in equations (7)-(9).

Similarly one can obtain the approximation for the shear forces

$$\overline{\mathbf{Q}}(\mathbf{x},s) = \mathbf{C}(\mathbf{x}) \sum_{a=1}^{n} [\phi^a(\mathbf{x})\mathbf{w}^{*a}(s) + \mathbf{F}^a(\mathbf{x})\hat{w}_3^a(s)], \tag{30}$$

where $\overline{\mathbf{Q}}(\mathbf{x},s) = \left[\overline{Q}_1(\mathbf{x},s),\, \overline{Q}_2(\mathbf{x},s)\right]^T$ and

$$\mathbf{C}(\mathbf{x}) = \begin{bmatrix} C_1(\mathbf{x}) & 0 \\ 0 & C_2(\mathbf{x}) \end{bmatrix}, \quad \mathbf{F}^a(\mathbf{x}) = \begin{bmatrix} \phi^a_{,1} \\ \phi^a_{,2} \end{bmatrix}.$$

Then, insertion of the MLS-discretized force fields (29) and (30) into the local boundary integral equations (18) and (19) yields the discretized local integral equations (LIEs)

$$\begin{aligned}
&\sum_{a=1}^{n} \left[\int_{L_s^i + \Gamma_{sw}^i} \mathbf{N}_\alpha(\mathbf{x})\mathbf{B}_\alpha^a(\mathbf{x}) d\Gamma \right. \\
&\left. - \int_{\Omega_s^i} \left(\mathbf{C}(\mathbf{x}) + \mathbf{E}\frac{\rho h^3(\mathbf{x})}{12} s^2 \right) \phi^a(\mathbf{x}) d\Omega \right] \mathbf{w}^{*a}(s) \\
&- \sum_{a=1}^{n} \hat{w}_3^a(s) \int_{\Omega_s^i} \mathbf{C}(\mathbf{x})\mathbf{F}^a(\mathbf{x}) d\Omega \\
&= \int_{L_s^i + \Gamma_{sM}^i} \overline{\mathbf{H}}(\mathbf{x},s) d\Gamma - \int_{\Gamma_{sM}^i} \tilde{\overline{\mathbf{M}}}(\mathbf{x},s) d\Gamma \\
&\qquad - \int_{\Omega_s^i} \overline{\mathbf{R}}(\mathbf{x},s) d\Omega, \quad (31)
\end{aligned}$$

$$\begin{aligned}
&\sum_{a=1}^{n} \left(\int_{\partial\Omega_s^i} \mathbf{C}_n(\mathbf{x})\phi^a(\mathbf{x}) d\Gamma \right) \mathbf{w}^{*a}(s) + \sum_{a=1}^{n} \hat{w}_3^a(s) \\
&\left(\int_{\partial\Omega_s^i} \mathbf{C}_n(\mathbf{x})\mathbf{F}^a(\mathbf{x}) d\Gamma - \int_{\Omega_s^i} \rho s^2 h(\mathbf{x})\phi^a(\mathbf{x}) d\Omega \right) \\
&\qquad = - \int_{\Omega_s^i} \overline{R}_3(\mathbf{x},s) d\Omega, \quad (32)
\end{aligned}$$

in which

$$\mathbf{E} = \begin{pmatrix} 1 & 0 \\ 0 & 1 \end{pmatrix},$$

$$\mathbf{C}_n(\mathbf{x}) = (n_1,\, n_2) \begin{pmatrix} C_1 & 0 \\ 0 & C_2 \end{pmatrix} = (C_1 n_1,\, C_2 n_2).$$

Equations (31) and (32) are considered on the subdomains adjacent to the interior nodes $\mathbf{x}^i$ as well as to the boundary nodes on Γ_{sM}^i.

For the source point $\mathbf{x}^i$ located on the global boundary Γ the boundary of the subdomain $\partial\Omega_s^i$ is decomposed into L_s^i and Γ_{sM}^i (part of the global boundary with prescribed bending moment) according to Fig. 3.

It should be noted here that there are neither Lagrange multipliers nor penalty parameters introduced into the local weak forms (13) and (14) because the essential boundary conditions on Γ_{sw}^i (part of the global boundary with prescribed rotations or displacements) can be imposed directly, using the interpolation approximation (24)

$$\sum_{a=1}^{n} \phi^a(\mathbf{x}^i)\hat{\mathbf{w}}^a(s) = \tilde{\overline{\mathbf{w}}}(\mathbf{x}^i,s) \quad \text{for } \mathbf{x}^i \in \Gamma_{sw}^i, \tag{33}$$

where $\tilde{\overline{w}}(\mathbf{x}^i,s)$ is the Laplace-transform of the generalized displacement vector prescribed on the boundary Γ_{sw}^i. For a clamped plate all three vector components (rotations and deflection) are vanishing on the fixed edge, and eq. (33) is used at all the boundary nodes in such a case. However, for a simply supported plate only the third component of the displacement vector (deflection) is prescribed, while the rotations are unknown. Then, the entire equation (31) and the third component of eq. (33) are applied to the nodes lying on the global boundary. On those parts of the global boundary where no displacement boundary conditions are prescribed both local integral equations, (31) and (32), are applied.

The time-dependent values of rotations, displacements, moments, and shear forces are obtained from an inverse transform of the corresponding Laplace-transformed quantities. Thereby, great attention is paid to the numerical inversion of the Laplace transformation, since the inverse Laplace-transform is an ill-posed problem and

small truncation errors can be greatly magnified in the inversion process with yielding poor numerical results. In the present analysis, the sophisticated Stehfest's algorithm [Stehfest, 1970] is used for the numerical inversion.

4 Meshless local integral equations for heat conduction problems in plates

The heat conduction problem cannot be reduced to 2-D as it was made for the plate problem described by the Reissner-Mindlin theory. Therefore, the problem has to be analyzed as a 3-D problem generally. Consider a boundary value problem for the heat conduction problem in a continuously nonhomogeneous anisotropic medium, which is described by the governing equation:

$$\rho(\mathbf{x})c(\mathbf{x})\frac{\partial \theta}{\partial t}(\mathbf{x},t) = [k_{ij}(x)\theta_{,j}(\mathbf{x},t)]_{,i} + Q(\mathbf{x},t), \tag{34}$$

where $\theta(\mathbf{x},t)$ is the temperature field, $Q(\mathbf{x},t)$ is the density of body heat sources, k_{ij} is the thermal conductivity tensor, $\rho(\mathbf{x})$ is the mass density and $c(\mathbf{x})$ the specific heat.

Let the analyzed plate is denoted by Ω with the top and bottom surfaces S^+ and S^-, respectively. Arbitrary temperature or heat flux boundary conditions can be prescribed on all considered surfaces. The initial condition is assumed

$$\theta(\mathbf{x},t)|_{t=0} = \theta(\mathbf{x},0)$$

in the analyzed domain Ω.

The above stated problem has been recently solved by [Qian and Batra, 2005] by an approximate computational technique. The temperature field is expanded in the plate thickness direction by using Legendre polynomials as basis functions. The original 3-D problem is transformed into a set of 2-D problems there. In the present paper, a more general 3-D analysis based on the MLPG method is applied. The MLS approximation is used here. The approximations described in previous paragraph for 2-D problems are still valid with only modification of basis polynomials as

$$\mathbf{p}^T(\mathbf{x}) = [1,\ x_1,\ x_2,\ x_3], \quad \text{linear basis } m = 4,$$

$$\mathbf{p}^T(\mathbf{x}) = [1,\ x_1,\ x_2, x_3,\ (x_1)^2,\ (x_2)^2,\ (x_3)^2,$$
$$x_1x_2,\ x_1x_2,\ x_3x_2,\ x_1x_3,\ (x_1)^2x_3,$$
$$(x_2)^2x_3,\ (x_3)^2x], \quad \text{quadratic basis } m = 10. \tag{35}$$

Applying the Laplace transformation to the governing equation (34), one obtains

$$\left[k_{ij}(\mathbf{x})\overline{\theta}_{,j}(\mathbf{x},s)\right]_{,i} - \rho(\mathbf{x})c(\mathbf{x})s\overline{\theta}(\mathbf{x},s) = -\overline{F}(\mathbf{x},s), \tag{36}$$

where

$$\overline{F}(\mathbf{x},s) = \overline{Q}(\mathbf{x},s) + \theta(\mathbf{x},0)$$

is the redefined body heat source in the Laplace-transform domain with initial boundary condition for temperature and s is the Laplace-transform parameter.

Again the weak form is constructed over local sub-domains Ω_s, which is a small sphere taken for each node inside the global domain. The local weak form of the governing equation (36) for $\mathbf{x}^a \in \Omega_s^a$ can be written as

$$\int_{\Omega_s^a} \Big[\left(k_{lj}(\mathbf{x})\overline{\theta}_{,j}(\mathbf{x},s)\right)_{,l} - \rho(\mathbf{x})c(\mathbf{x})s\overline{\theta}(\mathbf{x},s) + \overline{F}(\mathbf{x},s) \Big] \theta^*(\mathbf{x})d\Omega = 0, \tag{37}$$

where $\theta^*(\mathbf{x})$ is a weight (test) function.

Applying the Gauss divergence theorem to Eq. (37) we obtain

$$\int_{\partial\Omega_s^a} \overline{q}(\mathbf{x},s)\theta^*(\mathbf{x})d\Gamma - \int_{\Omega_s^a} k_{lj}(\mathbf{x})\overline{\theta}_{,j}(\mathbf{x},s)\theta^*_{,l}(\mathbf{x})d\Omega - \int_{\Omega_s^a} \rho(\mathbf{x})c(\mathbf{x})s\overline{\theta}(\mathbf{x},s)\theta^*(\mathbf{x})d\Omega + \int_{\Omega_s^a} \overline{F}(\mathbf{x},s)\theta^*(\mathbf{x})d\Omega = 0, \tag{38}$$

where $\partial\Omega_s^a$ is the boundary of the local subdomain and

$$\overline{q}(\mathbf{x},s) = k_{lj}(\mathbf{x})\overline{\theta}_{,j}(\mathbf{x},s)n_l(\mathbf{x}).$$

The local weak form (38) is a starting point to derive local boundary integral equations providing

an appropriate test function selection. If a Heaviside step function is chosen as the test function $\theta^*(\mathbf{x})$ in each sub-domain

$$\theta^*(\mathbf{x}) = \begin{cases} 1 & \text{at } \mathbf{x} \in \Omega_s^a \\ 0 & \text{at } \mathbf{x} \notin \Omega_s^a \end{cases}$$

the local weak form (38) is transformed into the following simple local boundary integral equation

$$\int_{\partial\Omega_s^a} \overline{q}(\mathbf{x},s)d\Gamma - \int_{\Omega_s^a} \rho(\mathbf{x})c(\mathbf{x})s\overline{\theta}(\mathbf{x},s)d\Omega = -\int_{\Omega_s^a} \overline{F}(\mathbf{x},s)d\Omega. \quad (39)$$

Equation (39) is recognized as the flow balance condition of the sub-domain. In stationary case there is no domain integration involved in the left hand side of this local boundary integral equation. If an assumption of zero body heat sources is made, a pure boundary integral formulation will be obtained.

The MLS is used for approximation of the heat flux $\overline{q}(\mathbf{x},s)$

$$\overline{q}^h(\mathbf{x},s) = k_{ij}n_i \sum_{a=1}^{n} \phi_{,j}^a(\mathbf{x})\hat{\theta}^a(s).$$

Substituting the MLS-approximations into the local integral equation (39) the system of algebraic equations is obtained

$$\sum_{a=1}^{n} \left(\int_{L_s+\Gamma_{sp}} \mathbf{n}^T\mathbf{K}\mathbf{P}^a(\mathbf{x})d\Gamma - \int_{\Omega_s} \rho cs\phi^a(\mathbf{x})d\Gamma \right) \hat{\theta}^a(s) = -\int_{\Gamma_{sq}} \tilde{\overline{q}}(\mathbf{x},s)d\Gamma - \int_{\Omega_s} \overline{R}(\mathbf{x},s)d\Omega, \quad (40)$$

at interior nodes as well as to the boundary nodes with prescribed heat flux on Γ_{sq}. In Eq. (40), we have used the notations

$$\mathbf{K} = \begin{bmatrix} k_{11} & k_{12} & k_{13} \\ k_{12} & k_{22} & k_{23} \\ k_{13} & k_{23} & k_{33} \end{bmatrix}, \quad \mathbf{P}^a(\mathbf{x}) = \begin{bmatrix} \phi_{,1}^a \\ \phi_{,2}^a \\ \phi_{,3}^a \end{bmatrix}, \quad (41)$$

$\mathbf{n}^T = (n_1, n_2, n_3)$.

The time dependent values of the transformed quantities can be obtained by an inverse Laplace-transform. In the present analysis, the Stehfest's inversion algorithm [Stehfest, 1970] is used.

5 Numerical examples

In this section, numerical results are presented for plates under thermal loading. In order to test the accuracy, the numerical results obtained by the present method are compared with the results provided by the FEM-ANSYS code using a very fine mesh. Clamped and simply supported square plates are analysed. In all numerical calculations, the plates with homogeneous and/or FGM properties are considered.

5.1 Simply supported square plate

We first consider a simply supported square plate with a side-length $a = 0.254m$ and the plate thicknesses $h/a = 0.05$. On the top surface of the plate a uniformly distributed temperature $\theta = 1^0$ is considered. The bottom surface is kept at vanishing temperature. In the first case homogeneous and isotropic material parameters are considered: Young's moduli $E_1 = E_2 = 0.6895 \cdot 10^{10}\,\mathrm{N/m^2}$, Poisson's ratios $\nu_{21} = \nu_{12} = 0.3$, and the thermal expansion coefficients $\alpha_{11} = \alpha_{22} = 1 \cdot 10^{-5}\,\mathrm{deg}^{-1}$. The used shear moduli correspond to Young's modulus E_2, namely, $G_{12} = G_{13} = G_{23} = E_2/2(1+\nu_{12})$.

For the purpose of error estimation and convergence studies the Sobolev norm is calculated. The relative error of the deflection is defined as

$$r = \frac{\left\| w_3^{num} - w_3^{exact} \right\|}{\left\| w_3^{exact} \right\|}, \quad (42)$$

where

$$\|w_3\| = \left(\int_{\Omega} w_3^2 d\Omega \right)^{1/2}.$$

The relative error for the bending moments is defined similarly. As the "exact" solution, Boley and Weiner (1960) results are used, since the plate is

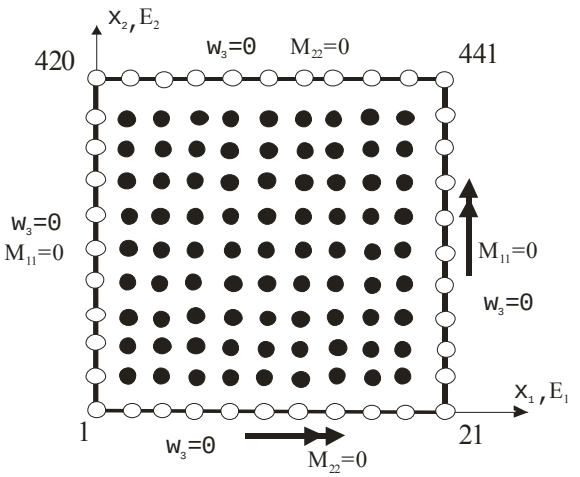

Figure 4: Node distribution for numerical analyses of a simply supported square plate

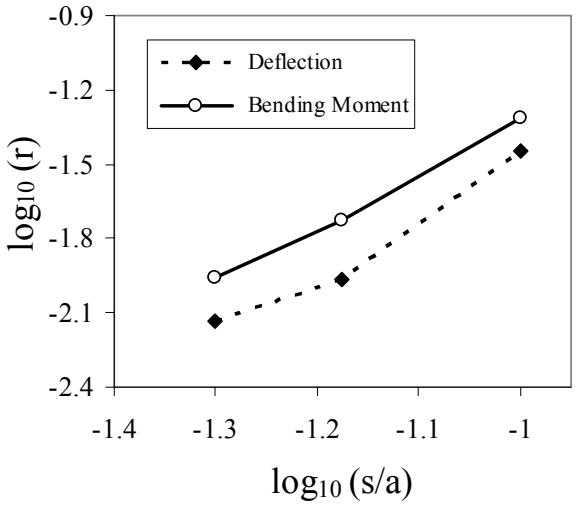

Figure 5: Relative errors and convergence rates for the central deflection and the bending moment of a simply supported plate

sufficiently thin and Kirchhoff theory can be applied. The analytical expressions for plate deflection and bending moments are given as

$$w_3(x_1,x_2) = \frac{\alpha\Delta\theta(1+\nu)4a^2}{\pi^3 h} \sum_{m=1,3,5...}^{\infty} \frac{\sin\frac{m\pi x_1}{a}}{m^3}\left(1-\frac{ch\frac{m\pi x_2}{a}}{ch\alpha_m}\right),$$

$$M_{11}(x_1,x_2) = \frac{4D\alpha\Delta\theta(1-\nu^2)}{\pi h} \sum_{m=1,3,5...}^{\infty} \frac{\sin\frac{m\pi x_1}{a} ch\frac{m\pi x_2}{a}}{mch\alpha_m},$$

$$M_{22}(x_1,x_2) = \frac{D\alpha\Delta\theta(1-\nu^2)}{h} - \frac{4D\alpha\Delta\theta(1-\nu^2)}{\pi h} \sum_{m=1,3,5...}^{\infty} \frac{\sin\frac{m\pi x_1}{a} ch\frac{m\pi x_2}{a}}{mch\alpha_m}, \quad (43)$$

where D is the flexural rigidity $D = Eh^3/12(1-\nu^2)$ and $\Delta\theta$ denotes a temperature difference between top and bottom plate surfaces. A linear temperature distribution is considered between both plate surfaces.

To study the convergence of the method, three regular node distributions with 121, 256, and 441 nodes, respectively, are used for the MLS approximation. For a regular node distribution (see Fig. 4), the density of the nodes can be characterized by the distance of two neighbouring nodes s. The relative errors and the convergence rates for the central deflection and bending moment are given in Fig. 5. The convergence rates for both quantities are almost the same. The relative error for the central deflection is a little bit lower than for the bending moment. For the finest node distribution with total 441 nodes the relative error for the central deflection is 0.56% and for the bending moment 0.85%, which confirms that the present numerical method is highly accurate. The circular subdomain is chosen as $r_{loc} = 0.4s$ and the radius of the support domain for node a is $r^a = 4r_{loc}$. Smaller values of the support domain lead to lower approximation accuracy, and larger values of the support domain prolong the computational time for the evaluation of the shape functions. The value of the radius of the support domain has been optimized on numerical experiments. Nie et al (2006) developed an efficient approach to find the optimal radius of support of radial weight functions used in MLS approximation.

The variation of the deflection with the x_1 - coordinate at x_2= a/2 of the plate is presented in

Fig. 6. The deflection is normalized to the plate thickness. One can observe a very good agreement of the present and analytical results. The FEM-ANSYS results have been obtained by 400 quadrilateral eight-node elements.

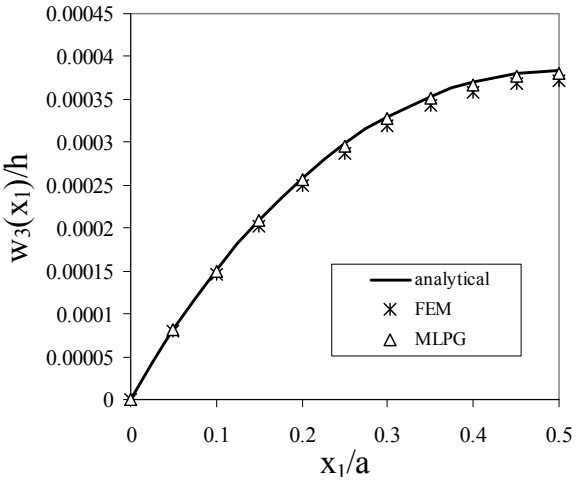

Figure 6: Variation of the deflection with the x_1 -coordinate for a simply supported isotropic square plate

The variation of the bending moment M_{11} is shown in Fig. 7. The bending moment at the center of the plate $M_{11}^{iso}(a/2) = 0.4634$ Nm is used as a normalized parameter. Again a very good agreement of results is observed.

Next, orthotropic mechanical properties of the plate are considered with Young's moduli $E_2 = 0.6895 \cdot 10^{10}$ N/m^2, $E_1 = 2E_2$, Poisson's ratios $\nu_{21} = 0.15$, $\nu_{12} = 0.3$. The variation of the deflection with the x_1-coordinate at $x_2 = a/2$ of the plate is presented in Fig. 8 with assuming isotropic thermal expansion coefficients. Opposite to mechanical load case [Sladek et al. 2007] the deflection is not reduced in the orthotropic plate as compared with the isotropic plate. It is due to increasing equivalent load for orthotropic plate at the same temperature distributions in both cases.

The variations of the bending moment M_{11} for orthotropic plate are presented in Fig. 9. We consider orthotropic properties for Young's moduli and for thermal expansion coefficients either isotropic or orthotropic. The bending moments are normalized by the central value for an isotropic plate. One can observe that orthotropic material properties of thermal expansion coefficient have a strong influence on the bending moment values.

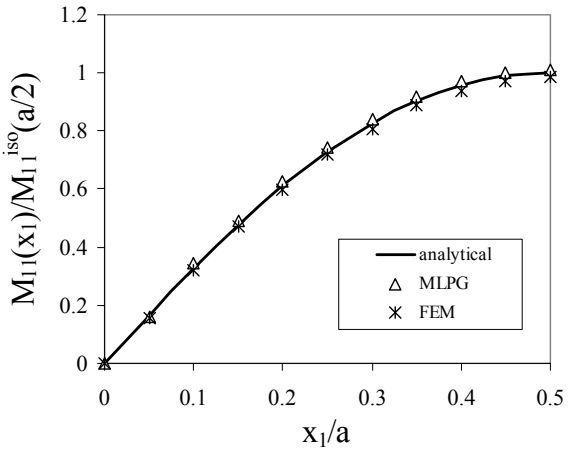

Figure 7: Variation of the bending moment with the x_1 -coordinate for a simply supported isotropic square plate

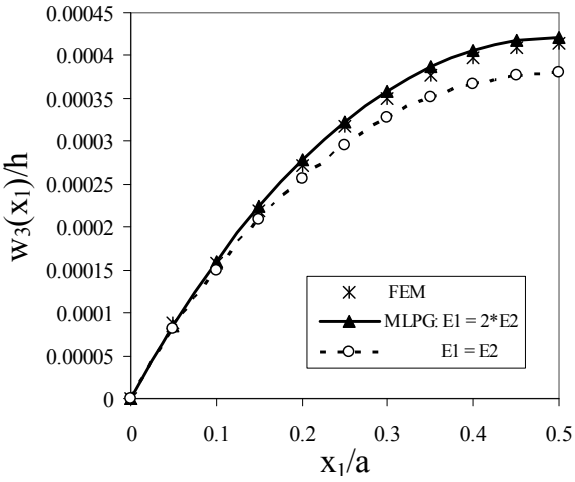

Figure 8: Influence of orthotropic material properties on the plate deflection

Next, functionally graded material properties through the plate thickness are considered. The following isotropic material parameters on top side of the plate are used in numerical analysis: Young's moduli $E_{1t} = E_{2t} = 0.6895 \cdot 10^{10}$N/m^2

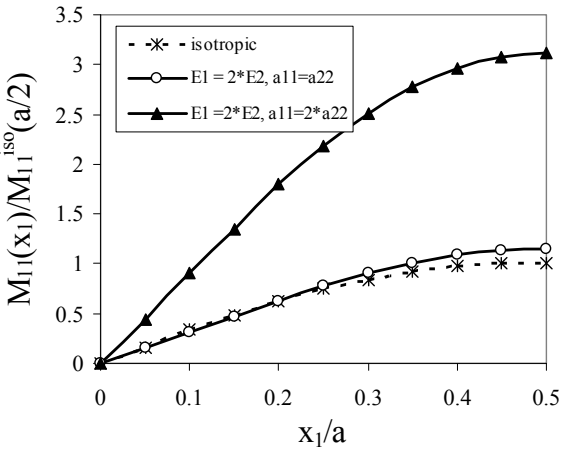

Figure 9: Variation of the bending moment with the x_1-coordinate for a simply supported orthotropic square plate

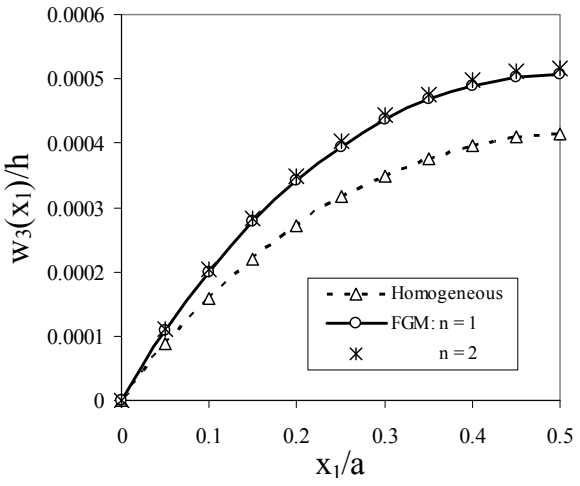

Figure 10: Variation of the deflection with the x_1 -coordinate for a simply supported isotropic square plate with FGM properties

, Poisson's ratios $\nu_{12} = \nu_{21} = 0.3$. Linear and quadratic variations of volume fraction V defined in equation (6) are considered here, and Young's moduli on the bottom side are: $E_{1b} = E_{2b} = E_{1t}/2$. The variation of deflections with the x_1 -coordinate is given in Fig. 10. Since Young's modulus on the bottom side is considered to be smaller than on the top one, deflection for FGM plate is larger than for homogenenous plate with material properties corresponding to the top side, $E_{2t} = 0.6895 \cdot 10^{10}\,\mathrm{N/m^2}$. In both linear and quadratic variations of Young's moduli the same surface values are considered. One can observe in Fig. 10 that the profile of the variation of material properties has negligible influence on the deflection. But the deflection is influenced by the surface values of material parameters on the bottom and top sides of the plate.

The variation of the bending moment M_{11} is presented in Fig. 11. Here, the bending moments are normalized by the central bending moment value corresponding to a homogeneous isotropic plate $M_{11}^{iso}(a/2) = 0.4634\,\mathrm{Nm}$. The profile of the variation of material properties through the plate thickness as well as their surface values has practically no influence on the bending moment. The bending moments in homogeneous and FGM plates are almost the same. Minimal differences between them are caused by numerical inaccuracies.

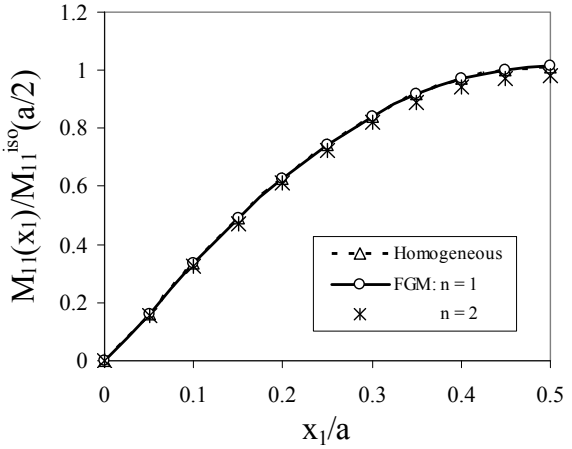

Figure 11: Variation of the bending moment with the x_1 -coordinate for a simply supported isotropic square plate with FGM properties

In the next example a thermal shock $\theta = H(t-0)$ with Heaviside time variation is applied on the top surface of the plate. If the ends of the plate are thermally insulated, a uniform temperature distribution on plate surfaces is given. The bottom surface is thermally insulated too. In such a case the temperature distribution is given by [Carslaw and

Jaeger, 1959]

$$\theta(x_3,t) = 1 - \frac{4}{\pi}\sum_{n=0}^{\infty}\frac{(-1)^n}{2n+1}\exp\left[-\frac{(2n+1)^2\pi^2\kappa t}{4h^2}\right] \cos\frac{(2n+1)\pi x_3}{2h}, \quad (44)$$

where diffusivity coefficient $\kappa = k/\rho c$, with thermal conductivity $k = 100\,\mathrm{W/mdeg}$, mass density $\rho = 7500\,\mathrm{kg/m^3}$ and specific heat $c = 400\,\mathrm{Ws/kgdeg}$. Isotropic material parameters and the thermal expansion coefficients are considered.

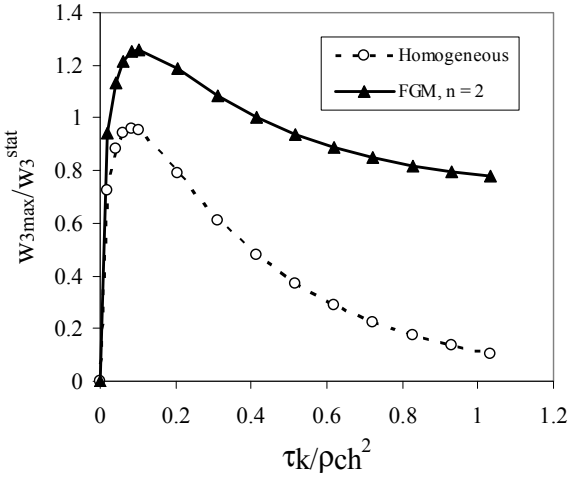

Figure 12: Time variation of the central deflection in the plate with vanishing heat flux

Homogeneous and FGM properties with n=2 are considered here. Numerical results for the central plate deflection are presented in Fig. 12. Deflections are normalized by the central deflection corresponding to stationary thermal distribution with $\theta = 1\,\mathrm{deg}$ on the top plate surface and vanishing temperature on the bottom surface. For homogeneous material properties the corresponding stationary deflection is $w_3^{stat} = 0.4829 \cdot 10^{-5}\,\mathrm{m}$. One can observe that in the whole time interval deflection for a homogeneous plate is lower than in a stationary case. The stiffness of the FGM plate is lower than for a homogeneous one.

For homogeneous plate the deflection approaches zero for late time instants. This is opposite to FGM plate. The bending moment at the center

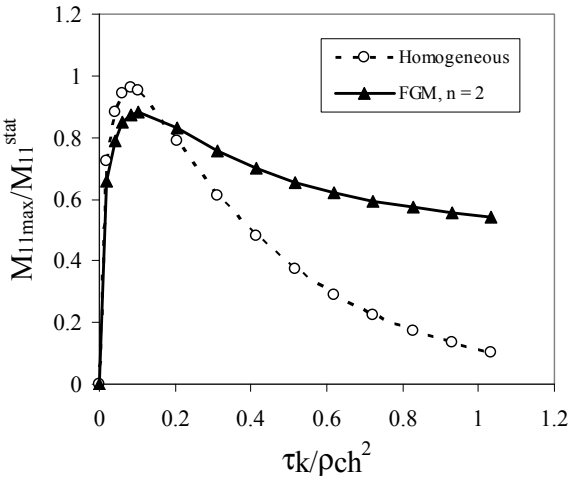

Figure 13: Time variation of the bending moment

of the plate $M_{11}^{stat} = 0.4699\,\mathrm{Nm}$ is used as a normalized parameter in Fig. 13. The peak values of the bending moments for both homogeneous and FGM plates are almost the same. Since the deflection is not vanishing for late time instants for the FGM plate, the bending moment is finite too.

5.2 Clamped square plate

Let us consider a clamped square plate with the same geometrical and material parameters as in the above analyzed simply supported plate. Also the same nodal distribution is used in the numerical analysis. A uniform distribution of temperature on the top side of the plate cannot be considered here, since it is leading to vanishing deflections [Boley and Weiner, 1960]. Therefore, we have considered following distribution of temperature on top surface of the plate:

$$\theta(x_1,x_2) = \sin\frac{\pi x_1}{a}\sin\frac{\pi x_2}{a}. \quad (45)$$

The bottom side of the plate is kept at vanishing temperature. A linear variation of temperature through the plate thickness is assumed. Both variants of isotropic and orthotropic material properties are considered here.

The variation of deflections with the x_1 - coordinate is given in Fig. 14. Counterpart to a simply supported plate the values of deflections

are independent on the ratio of Young's moduli in orthotropic material for a clamped plate. Increasing Young's modulus enlarges the thermal forces and flexural rigidity of the plate. Both effects are mutually eliminated in the deformation of plate. One can observe a good agreement of present and FEM results for both isotropic and orthotropic plates.

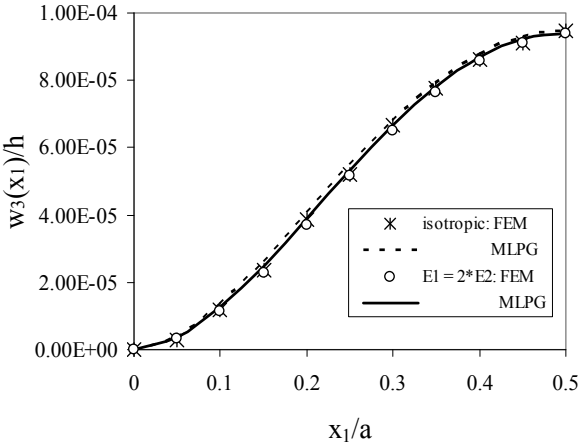

Figure 14: Variation of the deflection with the x_1 -coordinate for a clamped homogeneous square plate

The variation of the bending moment M_{11} is presented in Fig. 15. Here, the bending moments are normalized by the central bending moment value corresponding to a homogeneous isotropic plate. Larger bending moments at the fixed part of the orthotropic plate are caused by larger thermal forces. Orthotropic properties of thermal expansion coefficients have here a similar effect on the bending moment as the orthotropic mechanical material properties.

Next, functionally graded material properties through the plate thickness are considered. The variation of material properties for the FGM plate is here the same as for a simply supported plate analyzed in the previous example. The variation of deflections with the x_1 -coordinate is given in Fig. 16. Since Young's modulus on the bottom side is considered to be smaller than on the top one, deflection for the FGM plate is larger than for homogenenous plate with material properties

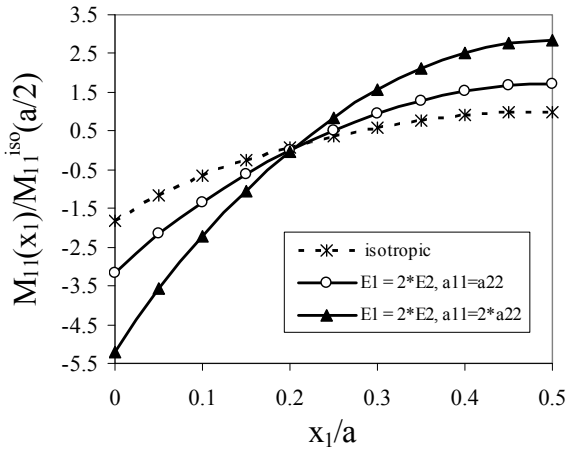

Figure 15: Variation of the bending moment with the x_1 -coordinate for a clamped homogeneous square plate

corresponding to the top side. The influence of gradation of material properties on the deflection of a clamped plate is similar to that in the simply supported plate.

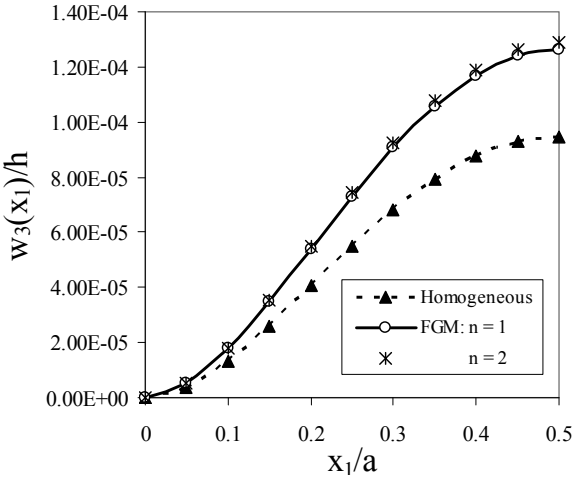

Figure 16: Variation of the deflection with the x_1 -coordinate for a clamped isotropic square plate with FGM properties

The variation of the bending moment M_{11} is presented in Fig. 17. Again the variation of material properties through the plate thickness has practically no influence on the bending moment.

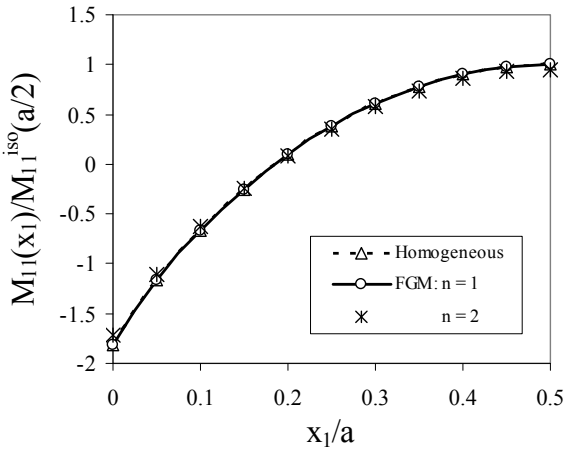

Figure 17: Variation of the bending moment with the x_1 -coordinate for a clamped isotropic square plate with FGM properties

The bending moments in homogeneous and FGM plates are almost the same.

6 Conclusions

A meshless local Petrov-Galerkin method is applied to plate bending problems described by the Reissner-Mindlin theory. Both stationary and thermal shock loads are considered. The variation of material properties through the plate thickness can be arbitrary. The influence of the shear deformation in the Reissner-Mindlin theory on the plate deflection is analysed. The Laplace-transform technique is applied to eliminate the time variable in the coupled governing differential equations of the Reissner-Mindlin theory. The use of the Laplace-transform in forced vibration analysis converts the dynamic problem to a quasi static problem. The analyzed domain is divided into small overlapping circular subdomains. A unit step function is used as the test function in the local weak-form. The derived local boundary-domain integral equations are nonsingular. The moving least-squares (MLS) scheme is adopted for approximating the physical quantities. The proposed method is a truly meshless method, which requires neither domain elements nor background cells in either the interpolation or the integration.

It is demonstrated numerically that the quality of the results obtained by the proposed MLPG method is very good. The degree of the agreement of our numerical results with those obtained by the FEM-ANSYS computer code ranges from good to excellent. Random location of nodes should be considered for a general boundary value problems. In illustrative examples only simple problems are analysed. Then, a regular node distribution has been used. However, an efficient node generator is required to be developed for further progress of the method.

Acknowledgement: The authors acknowledge the support by the Slovak Science and Technology Assistance Agency registered under number APVV-51-021205, the Slovak Grant Agency VEGA-2/6109/27, VEGA-1/4128/07, and the EPSRC research grant (U.K.) EP/E050573/1.

References

Andreaus, U.; Batra, R.C.; Porfiri, M. (2005): Vibrations of cracked Euler-Bernoulli beams using Meshless Local Petrov-Galerkin (MLPG) method. *CMES: Computer Modeling in Engineering & Sciences*, 9 (2): 111-131.

Atluri, S. N.; Shen, S. (2002): *The Meshless Local Petrov-Galerkin (MLPG) Method*, Tech Science Press.

Atluri, S. N. (2004): *The Meshless Method , (MLPG) For Domain & BIE Discretizations*, Tech Science Press.

Atluri, S.N.; Han, Z.D.; Shen, S. (2003): Meshless local Petrov-Galerkin (MLPG) approaches for solving the weakly-singular traction & displacement boundary integral equations. *CMES: Computer Modeling in Engineering & Sciences*, 4: 507-516.

Atluri, S.N.; Shen, S. (2005): Simulation of a 4^{th} order ODE: Illustartion of various primal & mixed MLPG methods. *CMES: Computer Modeling in Engineering & Sciences*, 7 (3): 241-268.

Atluri, S.N.; Liu, H.T.; Han, Z.D. (2006a): Meshless local Petrov-Galerkin (MLPG) mixed collocation method for elasticity problems. *CMES: Computer Modeling in Engineering &*

Sciences, 14 (3): 141-152.

Atluri, S.N.; Liu, H.T.; Han, Z.D. (2006b): Meshless local Petrov-Galerkin (MLPG) mixed finite difference method for solid mechanics. *CMES: Computer Modeling in Engineering & Sciences*, 15 (1): 1-16.

Bapu Rao, M.N. (1979): Thermal bending of thick rectangular plates. *Nuclear Engineering and Design,* 54: 115-118.

Belytschko, T.; Krogauz, Y.; Organ, D.; Fleming, M.; Krysl, P. (1996): Meshless methods; an overview and recent developments. *Comp. Meth. Appl. Mech. Engn.*, 139: 3-47.

Boley, B.A.; Weiner J.H. (1960): *Theory of Thermal Stresses*, John Wiley and Sons, New York.

Carslaw, H.S.; Jaeger, J.C. (1959): *Conduction of Heat in Solids*, Clarendon, Oxford.

Ching, H.K.; Chen, J.K. (2006): Thermomechanical analysis of functionally graded composites under laser heating by the MLPG method. *CMES: Computer Modeling in Engineering & Sciences*, 13 (3): 199-217.

Das, M.C.; Rath, B.K. (1972): Thermal bending of moderately thick rectangular plates. *AIAA Journal*, 10: 1349-1351.

De Leon, S.; Paris, F. (1987): Analysis of thermal stresses in plates with boundary element method. *Engineering Analysis*, 4: 199-203.

Han, Z.D.; Atluri, S.N. (2004a): Meshless local Petrov-Galerkin (MLPG) approaches for solving 3D problems in elasto-statics. *CMES: Computer Modeling in Engineering & Sciences*, 6: 169-188.

Han, Z.D.; Atluri, S.N. (2004b): A meshless local Petrov-Galerkin (MLPG) approach for 3-dimensional elasto-dynamics. *CMC: Computers, Materials & Continua*, 1: 129-140.

Han, Z.D.; Rajendran, A.N.; Atluri, S.N. (2005): Meshless Local Petrov-Galerkin (MLPG) approaches for solving nonlinear problems with large deformations and rotations. *CMES: Computer Modeling in Engineering & Sciences*, 10 (1): 1-12.

Han, Z.D.; Liu, H.T.; Rajendran, A.N.; Atluri, S.N. (2006): The applications of Meshless Local Petrov-Galerkin (MLPG) approaches in high-speed impact, penetration and perforation problems. *CMES: Computer Modeling in Engineering & Sciences*, 14 (2): 119-128.

Gao, L.; Liu, K.; Liu, Y. (2006): applications of MLPG method in dynamic fracture problems. *CMES: Computer Modeling in Engineering & Sciences*, 12 (3): 181-195.

Jarak, T.; Soric, J.; Hoster, J. (2007): Analysis of shell deformation responses by the Meshless Local Petrov-Galerkin (MLPG) approach. *CMES: Computer Modeling in Engineering & Sciences*, 18 (3): 235-246.

Johnson, J.N.; Owen, J.M. (2007): A meshless Local Petrov-Galerkin method for magnetic diffusion in non-magnetic conductors. *CMES: Computer Modeling in Engineering & Sciences*, 22 (3): 165-188.

Kamiya, N.; Sawaki Y.; Nakamura, Y. (1981): Thermal bending analysis by boundary integral equation method. *Mechanics Research Communications*, 8: 369-373.

Lancaster, P.; Salkauskas, T. (1981): Surfaces generated by moving least square methods, *Math. Comput.*, 37: 141-158.

Laura, P.A.A.; Rossit, C.A. (1999): Thermal bending of thin, anisotropic, clamped elliptic plates, *Ocean Engineering*, 29: 485-488.

Lekhnitskii, S.G. (1963): *Theory of Elasticity of an Anisotropic Body.* Holden Day.

Lin, R.M.; Lim, M.K.; Du, H. (1994): Large deflection analysis of plates under thermal loading. *Comp. Meth. Appl. Mech. Engn.*, 117: 381-390.

Long, S.Y.; Atluri, S.N. (2002): A meshless local Petrov Galerkin method for solving the bending problem of a thin plate. *CMES: Computer Modeling in Engineering & Sciences*, 3: 11-51.

Ma, Q.W. (2005): MLPG method based on Rankine source solution for simulating non-linear water waves. *CMES: Computer Modeling in Engineering & Sciences*, 9 (2): 193-209.

Ma, Q.W. (2007): Numerical generation of freak waves using MLPG-R and QALE-FEM methods. *CMES: Computer Modeling in Engineering & Sciences*, 18 (3): 223-234.

Ma, Q.W. (2008): A new meshless interpolation scheme for MLPG-R method. *CMES: Computer Modeling in Engineering & Sciences*, 23 (2): 75-89.

Marguerre, K. (1935): Thermoelastic plate equations. *Z. Ang. Math. und Mech.*, 15: 369-380.

Miyamoto, Y.; Kaysser, W.A.; Rabin, B.H.; Kawasaki, A.; Ford, R.G. (1999): *Functionally Graded Materials; Design, Processing and Applications*, Kluwer Academic Publishers, Dordrecht.

Mikhailov, S.E. (2002): Localized boundary-domain integral formulations for problems with variable coefficients. *Engn. Analysis with Boundary Elements*, 26: 681-690.

Mindlin, R.D. (1951): Influence of rotary inertia and shear on flexural motions of isotropic, elastic plates. *Journal of Applied Mechanics ASME*, 18: 31-38.

Nayroles, B.; Touzot, G.; Villon, P. (1992): Generalizing the finite element method. *Computational Mechanics*, 10: 307-318.

Nie, Y.F.; Atluri, S.N.; You, C.W. (2006): The optimal radius of the support of radial weights used in Moving Least Squares approximation. *CMES: Computer Modeling in Engineering & Sciences*, 12 (2): 137-147.

Pecher, R.; Elston, S.; Raynes, P. (2006): Meshfree solution of Q-tensor equations of nematostatics using the MLPG method. *CMES: Computer Modeling in Engineering & Sciences*, 13 (2): 91-101.

Praveen, G.N.; Reddy, J.N. (1998): Nonlinear transient thermoelastic analysis of functionally graded ceramic-metal plates, *Int. J. Solids and Structures*, 35: 4457-4476.

Providakis, C.P. (2007): The effect of internal support conditions to the elestoplastic transient response of Reissner-Mindlin plates. *CMES: Computer Modeling in Engineering & Sciences*, 18 (3): 247-258.

Qian, L.F.; Batra, R.C.; Chen, L.M. (2004): Analysis of cylindrical bending thermoelastic deformations of fuctionally graded plates by a meshless local Petrov-Galerkin method. *Computational Mechanics*, 33: 263-273.

Qian, L.F.; Batra R.C. (2005): Three-dimensional transient heat conduction in a functionally graded thick plate with a higher-order plate theory and a meshless local Petrov-Galerkin method. *Computational Mechanics*, 35: 214-226.

Reddy J.N. (1997): *Mechanics of Laminated Composite Plates: Theory and Analysis*. CRC Press, Boca Raton.

Reddy, J.N.; Hsu, Y.S. (1980): Effects of shear deformation and anisotropy on the thermal bending of layered composite plates, *Journal of Thermal Stresses*, 3: 475-493.

Reissner, E. (1946): Stresses and small displacements analysis of shallow shells-II, *Journal Math. Physics*, 25: 279-300.

Rolfes, R.; Noor, A.K.; Sparr, H. (1998): Evaluation of transverse thermal stresses in composite plates based on first-order shear deformation theory, *Computer Methods in Applied Mechanics and Engineering*, 167: 355-368.

Sellountos, E.J.; Vavourakis, V.; Polyzos, D. (2005): A new singular/hypersingular MLPG (LBIE) method for 2D elastostatics, *CMES: Computer Modeling in Engineering & Sciences*, 7: 35-48.

Shen, H.S. (2000): Nonlinear analysis of simply supported Reissner-Mindlin plates subjected to lateral pressure and thermal loading and resting on two-parameter elastic foundations. *Engineering Structures*, 23: 1481-1493.

Sladek, J.; Sladek, V.; Mang, H.A. (2002): Meshless formulations for simply supported and clamped plate problems. *Int. J. Num. Meth. Engn.*, 55: 359-375.

Sladek, J.; Sladek, V.; Mang, H.A. (2003): Meshless LBIE formulations for simply supported and clamped plates under dynamic load. *Computers and Structures*, 81: 1643-1651.

Sladek, J.; Sladek, V.; Krivacek, J.; Wen, P.; Zhang, Ch. (2007): Meshless Local Petrov-Galerkin (MLPG) method for Reissner-Mindlin plates under dynamic load. *Computer Meth. Appl. Mech. Engn.*, 196: 2681-2691.

Soric, J.; Li, Q.; Atluri, S.N. (2004): Mesh-

less local Petrov-Galerkin (MLPG) formulation for analysis of thick plates. *CMES: Computer Modeling in Engineering & Sciences*, 6: 349-357.

Stehfest, H. (1970): Algorithm 368: numerical inversion of Laplace transform. *Comm. Assoc. Comput. Mach.*, 13: 47-49.

Suetake, Y. (2006): Plate bending analysis by using a modified plate theory. *CMES: Computer Modeling in Engineering & Sciences,* 11 (3): 103-110.

Suresh, S.; Mortensen A. (1998): *Fundamentals of Functionally Graded Materials.* Institute of Materials, London.

Tauchert T.R. (1986) Thermal stresses in plates – statical problems, In *Thermal Stresses* (Hetnarski R.B. ed.), vol I. North Holland: New York, 23-137.

Tauchert T.R. (1987) Thermal stresses in plates – dynamical problems, In *Thermal Stresses* (Hetnarski R.B. ed.), vol II. North Holland: New York, 23-137.

Tauchert T.R. (1991): Thermally induced flexure, buckling and vibration of plates. *Applied Mechanics Reviews,* 44: 347-360.

Vel, S.S.; Batra, R.C. (2002): Exact solution for thermoelastic deformations of functionally graded thick rectangular plates. *AIAA Journal*, 40: 1421-1433.

Wen, P.H.; Hon, Y.C. (2007): Geometrically nonlinear analysis of Reissener-Mindlin plate by meshless computation. *CMES: Computer Modeling in Engineering & Sciences*, 21(3): 177-191.

Wu, X.H.; Shen, S.P.; Tao, W.Q. (2007): Meshless Local Petrov-Galerkin collocation method for two-dimensional heat conduction problems. *CMES: Computer Modeling in Engineering & Sciences*, 22 (1): 65-76.

Yuan, W.; Chen, P.; Liu, K. (2007): a new quasi-unsymmetric sparse linear systems solver for Meshless Local Petrov-Galerkin method (MLPG). *CMES: Computer Modeling in Engineering & Sciences*, 17 (2): 115-134.